Canadian Science Publishing

ARTICLE

Hydromechanical behaviour of two unsaturated silts: laboratory data and model predictions

Agostino Walter Bruno, Domenico Gallipoli, and Joao Mendes

Abstract: This paper presents the results from a campaign of unsaturated and saturated isotropic tests performed on two compacted silts of different coarseness, namely a clayey silt and a sandy silt, inside triaxial cells. Some tests involved an increase or a decrease of mean net stress at constant suction or an increase or a decrease of suction at constant mean net stress. Other tests involved an increase of mean net stress at constant water content with measurement of suction. During all tests, the void ratio and degree of saturation were measured to investigate the mechanical and retention behaviour of the soil. The experimental results were then simulated by the bounding surface hydromechanical model of A.W. Bruno and D. Gallipoli (2019. Computers and Geotechnics, **110**: 287–295. doi:10.1016/j.compgeo.2019.02.025), which was originally formulated to describe the behaviour of clays and clayey silts. Model parameters were calibrated against unsaturated tests including isotropic loading stages at constant water content with measurement of varying suction. Loading at constant water content is relatively fast and allows the simultaneous exploration of large ranges of mean net stress and suction, thus reducing the need of multiple experiments at distinct suction levels. Predicted data match well the observed behaviour of both soils, including the occurrence of progressive yielding and hysteresis, which extends the validation of this hydromechanical model to coarser soils. Specific features of the unsaturated soil behaviour, such as wetting-induced collapse, are also well reproduced.

Key words: unsaturated soils, hydromechanical behaviour, bounding surface plasticity, unsaturated triaxial testing, collapse–compression.

Résumé : Le but de la présente étude est de démontrer les résultats d'une campagne d'essais isotropes non saturés et saturés effectués sur deux limons compactés de granulométrie différente, à savoir un limon argileux et un limon sableux, à l'intérieur de cellules triaxiales. Dans le premier cas, il s'agissait d'une augmentation ou diminution de la contrainte nette moyenne pour une aspiration constante ou d'une augmentation ou diminution de l'aspiration pour une contrainte nette moyenne constante. La contrainte nette moyenne a été augmentée pour une teneur en eau constante avec une mesure de la succion. Au cours de tous les essais, le taux de vide et le degré de saturation ont été mesurés pour étudier le comportement mécanique et de rétention du sol. Les résultats expérimentaux ont ensuite été simulés par le modèle hydromécanique de surface limite de A.W. Bruno et D. Gallipoli (2019. Computers and Geotechnics, **110**: 287–295. doi:10.1016/j.compgeo.2019.02.025), initialement formulé pour décrire le comportement des argiles et des limons argileux. La calibration des paramètres du modèle a été réalisée à partir d'essais non saturés comprenant des étapes de chargement isotrope à teneur en eau constante avec mesure de la succion variable. Le chargement à teneur en eau constante est relativement rapide et permet l'exploration simultanée de larges gammes de contraintes nettes moyennes et de succion, réduisant ainsi le besoin d'expériences multiples à des niveaux de succion distincts. Les données prédites correspondent bien au comportement observé des deux sols, y compris l'apparition d'une déformation progressive et d'une hystérésis, ce qui étend la validation de ce modèle hydromécanique aux sols plus grossiers. Les caractéristiques spécifiques du comportement des sols non saturés, telles que l'effondrement induit par le mouillage, sont également bien reproduites. [Traduit par la Rédaction]

Mots-clés : sols non saturés, comportement hydromécanique, plasticité de la surface limite, essais triaxiaux non saturés, effondrement–compression.

Introduction

Geotechnical design often requires the prediction of the hydromechanical behaviour of unsaturated soils, as these make up a large proportion of earthworks including fills, embankments, and dams. Shallow natural soils also exist in a partly saturated state, which has important consequences on the stability of foundations, cuttings, and slopes.

Over the past decades, researchers have developed reliable techniques to measure the hydraulic and mechanical behaviour of unsaturated soils by upgrading standard equipment for saturated soils such as oedometers, shear boxes, and triaxial cells

Received 8 April 2021. Accepted 31 July 2021.

A.W. Bruno.* School of Engineering, Geotechnics and Structures, Newcastle University, Newcastle upon Tyne, UK.
D. Gallipoli. Dipartimento di Ingegneria Civile, Chimica e Ambientale, Università degli Studi di Genova, Genoa, Italy.
J. Mendes. Faculty of Engineering and Environment, Department of Mechanical & Construction Engineering, Northumbria University, Newcastle upon Tyne, UK.
Corresponding author: Agostino Bruno (email: agostinowalter.bruno@unige.it).
*Present address: Dipartimento di Ingegneria Civile, Chimica e Ambientale, Università degli Studi di Genova, Genoa, Italy.

(e.g., Gan et al. 1988; Delage et al. 1998; Cunningham et al. 2003; Tarantino and Tombolato 2005; Jotisankasa et al. 2007), or by designing new instrumentation such as pressure plates, psychrometers, and high-capacity tensiometers (e.g., Fredlund and Wong 1989; Ridley and Burland 1993; Tinjum et al. 1997; Mendes et al. 2008, 2019; Lourenço et al. 2008, 2011; Toll et al. 2013).

These experimental advances have in turn elicited the development of increasingly accurate material models. A milestone has been the definition of the soil–water retention curve linking uniquely the degree of saturation to pore water suction (e.g., Van Genuchten 1980; Fredlund and Xing 1994), which has found application not only in geotechnical engineering but also agriculture and hydrology (Siemens et al. 2014; Balzano et al. 2021). More complex retention laws have also been proposed to describe the effects of hysteresis, material fabric, and volumetric deformations on soil saturation (e.g., Gallipoli et al. 2003*a*; Nuth and Laloui 2008; Tarantino 2009; Romero et al. 2011), while mechanical laws have been formulated to describe the effect of pore water capillarity on soil stiffness, deformation, and strength (e.g., Alonso et al. 1990; Wheeler and Sivakumar 1995; Gallipoli et al. 2003*b*; Lim and Siemens 2016). In some instances, retention and mechanical laws have been combined into a single coupled hydromechanical framework (e.g., Wheeler et al. 2003; Khalili et al. 2008; Sun et al. 2008; Lloret-Cabot et al. 2013, 2017, 2018; Sun et al. 2016; Zhou et al. 2018).

Past research has tended to focus on the behaviour of unsaturated clays, while coarser soils have generally received less attention (Delage et al. 1996; Geiser et al. 2006; Oka et al. 2010; Zhao and Zhang 2014). A thorough understanding of coarser soils is, however, important because these materials are commonly encountered in geotechnical works (e.g., dams, embankments) and widely used in earth building (Bruno et al. 2017; Cuccurullo et al. 2018). This paper contributes to the investigation of the unsaturated behaviour of coarser soils by testing two different silts under isotropic conditions inside triaxial cells along a variety of stress paths that include (*i*) increase or decrease of mean net stress at constant suction, (*ii*) increase or decrease of suction at constant mean net stress, and (*iii*) increase of mean net stress at constant water content with the simultaneous measurement of suction. Recall that the mean net stress p_{net} is the difference between the mean total stress p and the pore air pressure u_a, whereas the suction s is the difference between the pore air pressure u_a and the pore water pressure u_w. Note that the present experimental campaign focuses on remoulded or compacted samples, whereas the characterisation of intact or undisturbed soils is outside the scope of this work.

Test results were used to calibrate the bounding surface model of Bruno and Gallipoli (2019), which predicts the hysteretic hydromechanical behaviour of unsaturated soils under isotropic stress states. The model accounts for the effect of hydraulic hysteresis and deformation on soil–water retention and, vice versa, for the effect of the degree of saturation and capillarity on deformation. Model parameters were calibrated against isotropic tests on unsaturated samples, which involved loading at constant water content with measurement of varying suction, followed by unloading at constant suction with measurement of varying water content. Note that loading at constant water content produces simultaneous variations of mean net stress and suction, which simplifies model calibration because it reduces the need of performing multiple tests at distinct suction levels. The calibrated model was finally employed to simulate the soil response during additional tests not used for selecting parameter values. The simulations show a good agreement between predicted and experimental data, including the occurrence of collapse–compression upon wetting. This confirms that the model of Bruno and Gallipoli (2019) is indeed capable of describing the behaviour of relatively coarse materials, such as sandy silts, in addition to the behaviour of fine soils.

Hydromechanical model

The hydromechanical model of Bruno and Gallipoli (2019) couples the hysteretic retention law for deformable soils of Gallipoli et al. (2015) with the hysteretic mechanical law for unsaturated soils of Gallipoli and Bruno (2017), which are both briefly summarised in this section.

The retention law accounts for the combined effect of void ratio e and matric suction s on the hysteretic variation of degree of saturation S_r by means of two distinct equations, i.e., one for wetting and one for drying (Gallipoli et al. 2015). Similarly, the mechanical law accounts for the effect of degree of saturation S_r and mean average skeleton stress $p' = p - u_a + S_r s$ (also known as Bishop's stress) on the hysteretic variation of void ratio e by means of two distinct equations, i.e., one for loading and one for unloading (Gallipoli and Bruno 2017). Each one of the wetting, drying, loading, and unloading equations originates from the integration of a differential constitutive law (Gallipoli et al. 2015; Gallipoli and Bruno 2017), and therefore, includes a constant of integration whose value must be determined by imposing a boundary condition. Table 1 summarises the above four equations together with the expressions of the respective constants of integration. Table 1 also lists the 12 parameters of the hydromechanical model, i.e., 7 parameters for the retention law and 5 parameters for the mechanical law.

The constants of integration C_w and C_d uniquely identify the wetting and drying paths, respectively, passing through a soil state characterised by suction s_0, void ratio e_0, and degree of saturation $S_{r,0}$. Similarly, the constants of integration C_l and C_u uniquely identify the loading and unloading paths, respectively, passing through a soil state characterised by void ratio e_0, mean average skeleton stress p'_0, and degree of saturation $S_{r,0}$. Further details about the derivation of both retention and mechanical laws, together with a discussion of the physical meaning of the corresponding parameters, can be found in Gallipoli et al. (2015) and Gallipoli and Bruno (2017), respectively.

The above retention and mechanical laws are coupled via the iterative algorithm of Bruno and Gallipoli (2019). According to this algorithm, the degree of saturation computed from the retention law is inserted into the mechanical law to calculate the corresponding value of void ratio, which is then inserted back into the retention law to calculate a new value of degree of saturation. This triggers a recursive process, which is repeated n times until the following two convergency criteria are simultaneously met

$$\left|\frac{S_{r,n} - S_{r,n-1}}{S_{r,n-1}}\right| \leq 0.001 \quad (1a)$$

$$\left|\frac{e_n - e_{n-1}}{e_{n-1}}\right| \leq 0.001 \quad (1b)$$

Once eqs. 1*a* and 1*b* are satisfied, the algorithm is assumed to have converged and the simulation moves to the next values of suction and mean net stress along the chosen path. Additional details about this iterative procedure can be found in Bruno and Gallipoli (2019).

This coupled hydromechanical framework has already been validated by Bruno and Gallipoli (2019) against laboratory data for fine soils, whereas in the present paper, the capabilities of the model are further tested against the behaviour of coarser materials.

Materials and methods

Material properties

The soils tested in the present work were provided by two brickwork factories, i.e., Nagen and Bouisset, in the region of Toulouse (France). The grain size distributions of both soils were

Table 1. Retention and mechanical laws.

	Equation and parameters
Retention law (Gallipoli et al. 2015)	
Wetting paths	$(S_r)_w = \left\langle 1 + \left\{ (se^{1/\lambda_s})^{\beta_w} / \omega_w^{\beta_w} \left[1 + C_w (se^{1/\lambda_s})^{\beta_w} \right] \right\}^{\lambda_s/\beta_w m_w} \right\rangle^{-m_w}$
Wetting path — constant of integration	$C_w = \left(1/\omega_w^{\beta_w}\right)\left({S_{r,0}}^{-1/m_w} - 1\right)^{-\beta_w m_w/\lambda_s} - 1/\left(s_0 e_0^{1/\lambda_s}\right)^{\beta_w}$
Drying paths	$(S_r)_d = \left\langle 1 + \left\{ \left[(se^{1/\lambda_s})^{\beta_d} + C_d \right] \Big/ \omega_d^{\beta_d} \right\}^{\lambda_s/\beta_d m_d} \right\rangle^{-m_d}$
Drying path — constant of integration	$C_d = {\omega_d}^{\beta_d}\left({S_{r,0}}^{-1/m_d} - 1\right)^{\beta_d m_d/\lambda_s} - \left(s_0 e_0^{1/\lambda_s}\right)^{\beta_d}$
Model parameters	λ_s, ω_w, m_w, β_w, ω_d, m_d, β_d
Mechanical law (Gallipoli and Bruno 2017)	
Loading paths	$e = \left[\left(p' {S_r}^{\lambda_r/\lambda_p} / \overline{p}_{ref} \right)^{\gamma} + C_l \right]^{-\lambda_p/\gamma}$
Loading paths — constant of integration	$C_l = e_0^{-\gamma/\lambda_p} - \left(p'_0 {S_{r,0}}^{\lambda_r/\lambda_p} / \overline{p}_{ref} \right)^{\gamma}$
Unloading paths	$e = C_u / \left(p' {S_r}^{\lambda_r/\lambda_p} \right)^{\kappa}$
Unloading paths — constant of integration	$C_u = e_0 \left(p'_0 {S_{r,0}}^{\lambda_r/\lambda_p} \right)^{\kappa}$
Model parameters	λ_p, λ_r, $\overline{p}_{ref}$, γ, κ

determined by wet sieving and sedimentation according to the norms XP P94-041 (AFNOR 1995*b*) and NF P 94-057 (AFNOR 1992), respectively. The plasticity properties of the fine fraction (i.e., the fraction passing through the 400 μm sieve) were determined according to the norm NF P94-051 (AFNOR 1993). The specific gravity of the soil grains, G_s, was instead measured by means of the pycnometer test according to the norm NF P 94-054 (AFNOR 1991). The clay activity, A (defined as the ratio between the plasticity index and the soil fraction smaller than 2 μm), is equal to 0.79 for the Nagen soil and 0.6 for the Bouisset soil, which classifies the former material as normally active and the latter material as inactive (Skempton 1953). This is also consistent with the mineralogical data provided by the suppliers, which indicate a predominantly illitic content with a small quantity of montmorillonite for the Nagen soil and a predominantly kaolinitic content for the Bouisset soil. Table 2 summarises the main properties of both materials.

The compaction curves, relating dry density ρ_d to water content w, were measured for both soils according to the procedure proposed by Sivakumar (1993), Sharma (1998), and Raveendiraraj (2009). Prior to compaction, the dry material was mixed with the desired amount of water using an electrical planetary blender for at least 3 min. The moist soil was left to equalise inside two plastic bags for a minimum of 24 h before being statically compacted (in 10 layers for the Nagen soil and 12 layers for Bouisset soil) inside a 50 mm diameter cylindrical mould with a constant vertical displacement rate of 1.5 mm/min until achieving a target pressure of 400 kPa. The diameter of each compacted sample was measured three times at different heights, while the height was measured three times at different angles. The volume of the sample was calculated from the average measurements of diameter and height, while the mass was recorded by a scale with a resolution of 0.01 g. The water content was calculated as the average of three measurements taken on specimens of about 50 g from the top, middle, and bottom of the sample, respectively, according to the norm NF P94-050 (AFNOR 1995*a*). The measured values of volume, mass, water content, and specific gravity were finally used to calculate the bulk density, dry density, porosity, and degree of saturation of the samples.

Figure 1 plots the measured values of dry density ρ_d versus water content w for both Nagen and Bouisset soils together with the respective interpolating curves. Inspection of Fig. 1 indicates that the Nagen soil exhibits lower values of the optimum water content and dry density (i.e., 12.75% and 1643 kg/m^3) than the Bouisset soil (i.e., 15.0% and 1839 kg/m^3). The optimum of the Nagen soil corresponds to a degree of saturation of 55%, which is slightly smaller than the values observed in similar soils, i.e., 65%–85% (Tatsuoka 2015). This difference can be explained by the relatively modest compaction energy applied in this work compared with the standard Proctor (Sharma 1998). The same feature is not observed for the Bouisset soil, which exhibits a finer grading and a higher retention capacity than the Nagen soil.

Table 2. Main material properties.

	Nagen	Bouisset
Grain size distribution		
Gravel, >2 mm (%)	0.4	0.0
Sand, 0.063–2 mm (%)	40.4	26.6
Silt, 0.002–0.063 mm (%)	42.9	41.9
Clay, <0.002 mm (%)	16.3	31.5
Plasticity properties		
Liquid limit, w_L (%)	33.0	35.5
Plastic limit, w_P (%)	20.1	16.7
Plasticity index, I_P (%)	12.9	18.8
Clay activity, A (—)	0.79	0.60
Specific gravity of soil grains		
Specific gravity, G_s (—)	2.66	2.65

Triaxial samples of 50 mm diameter and 100 mm height were produced by compacting both soils at water contents 4% lower than their respective optimum value, thus resulting in a dry density equal to 92% of the corresponding optimum level. Dry-of-optimum compaction was chosen because it induces a double porosity material fabric with a relatively low air-entry value of suction, which facilitates unsaturated testing (Delage et al. 1996; Tarantino and De Col 2008; Monroy et al. 2010; Casini et al. 2012).

The initial suction was recorded inside a triaxial cell, via the axis translation technique, on freshly compacted samples under a small mean net stress of 20 kPa and restrained pore water drainage. After ramping up the cell and pore air pressures to 950 and 930 kPa, respectively, the pore water pressure was measured and

Fig. 1. Static compaction curves of Nagen and Bouisset soils.

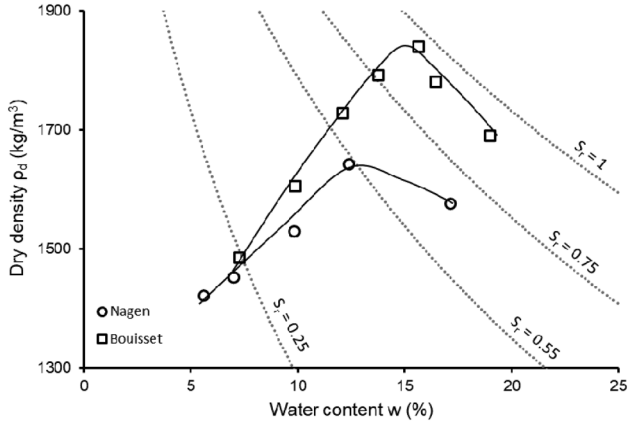

subtracted from the corresponding pore air pressure to calculate the soil suction. Table 3 summarises the average "as-compacted" properties of the triaxial samples of both materials.

Triaxial testing equipment

Unsaturated tests were performed by using two identical double-walled triaxial cells commercialised by the company VJ Tech. The volumetric deformation of the samples was measured by a volume change device, which was hydraulically connected to the inner cell. Suction was controlled (or measured) via the axis translation technique by two pumps imposing (or recording) the pore air and water pressures, respectively. The top and bottom faces of the sample were hydraulically connected to the pore water line through two saturated porous ceramic discs characterised by an air-entry value of 1500 kPa. A relatively high air-entry value was chosen to minimise pore air diffusion, and therefore, to avoid the formation of bubbles in the pore water line, which would affect measurements.

Each test consisted of a combination of the following stages: (*i*) increase or decrease of mean net stress at constant suction, (*ii*) increase or decrease of suction at constant mean net stress, and (*iii*) increase of mean net stress at constant water content with the simultaneous measurement of suction.

The mean net stress was increased with a rate of 2 kPa/h and decreased with a rate of 4 kPa/h, while suction was increased and decreased with a rate of 2 kPa/h. Following Al-Sharrad (2013), the mean net stress and suction were maintained constant at the end of each test stage, during a "rest" period, until both the specific volume, $v = 1 + e$, and the specific water volume, $v_w = 1 + wG_s$, changed less than 0.001 per day. Test stages involving an increase or a decrease of mean net stress or an increase of suction required rest periods of about 48 h, during which only small variations of v and v_w were observed. Conversely, test stages involving a decrease of suction required significantly longer rest periods of about 6 days, during which much larger variations of v and v_w were recorded, as discussed later.

Saturated tests were performed by using a standard triaxial cell commercialised by the company VJ Tech. Samples were preliminarily saturated by flushing water from bottom to top, followed by back-pressurisation up to 350 kPa under a low mean effective stress of about 5 kPa. After saturation, the mean effective stress was increased by augmenting the cell pressure with a rate of 2 kPa/h while maintaining the pore water pressure at 350 kPa. The pore water pressure was controlled by means of an automatic pump, which also served the purpose of recording the change of water content inside the sample. Given the saturated state of the soil, the volumetric deformations of the sample were directly computed from the recorded changes of water content.

Table 4 summarises the stages of all tests performed in this work and indicates whether the corresponding results were used for model calibration or validation.

Calibration of retention and mechanical laws

In principle, the above retention and mechanical laws can be calibrated by means of two alternative strategies. The first strategy consists in a simultaneous optimisation of all parameter values inside each law via a least square regression of experimental data. The second strategy consists instead in the interpolation of individual features of material behaviour depending on the physical meaning of each parameter. Bruno and Gallipoli (2019) adopted a hybrid calibration approach that combined the former strategy for the retention law with the latter strategy for the mechanical law. In the present work, instead, the former strategy has been adopted for selecting parameter values inside both retention and mechanical laws via the interpolation of results from tests on unsaturated samples subjected to constant water content loading followed by unloading at constant suction. Note that each constant water content loading path allows the simultaneous exploration of relatively large ranges of mean net stress and suction, which is particularly advantageous for model calibration.

The following sections describe the calibration of both retention and mechanical laws against the experimental data for Nagen and Bouisset soils.

Calibration of retention law

The seven parameters (i.e., λ_s, ω_w, β_w, m_w, ω_d, β_d, m_d) of the retention law were selected, at once, via a simultaneous least square regression of two tests for each soil, i.e., tests 1N and 2N for the Nagen soil and tests 1B and 2B for the Bouisset soil (Table 3). Each of these four tests consisted of a cycle of mean net stress with loading at constant water content followed by unloading at constant suction.

For the Nagen soil, test 1N (Fig. 2) involved an initial increase of mean net stress from 20 to 680 kPa at constant water content, followed by a reduction of mean net stress from 680 back to 20 kPa at constant suction of 210 kPa. During the loading stage, suction first increased from 210 to 354 kPa and then reduced back to 210 kPa. This behaviour is different from that observed during subsequent tests 2N, 1B, and 2B, where suction consistently reduced throughout loading at constant water content. The difference might have been caused by an accumulation of diffused air into the pore water line and the consequent formation of air bubbles affecting the measurement of pore water pressure. Note that test 1N was the first test of the experimental campaign, and for all subsequent tests, the pore water line was regularly flushed to prevent the potential formation of air bubbles. Test 2N (Fig. 3) started with an increase of mean net stress from 20 to 560 kPa at constant water content, which produced a reduction of suction from 550 to 330 kPa, followed by a reduction of mean net stress from 560 back to 20 kPa at constant suction of 330 kPa.

For the Bouisset soil, test 1B (Fig. 4) started with an increase of mean net stress from 20 to 830 kPa at constant water content, which produced a reduction of suction from the initial value of 220 to 55 kPa, followed by a reduction of mean net stress from 830 back to 20 kPa under a constant suction of 55 kPa. Test 2B (Fig. 5) started instead with an increase of mean net stress from 30 to 790 kPa at constant water content, which produced a suction drop from the initial value of 500 to 90 kPa, followed by a reduction of mean net stress from 790 back to 20 kPa at a constant suction of 90 kPa.

Figures 2–5 compare the experimental and calibrated variations of degree of saturation for tests 1N, 2N, 1B, and 2B. The grey and black labels, placed next to the measured and computed curves respectively, identify the start and end points of each test stage. The calibrated data were computed by using either the wetting or

Table 3. Properties of triaxial samples after compaction.

	Water content, w (%)	Bulk density, ρ_b (kg/m^3)	Dry density, ρ_d (kg/m^3)	Porosity, n (—)	Void ratio, e (—)	Degree of saturation, S_r (%)	Suction, s (kPa)
Nagen	8.75	1648	1515	0.430	0.756	30.8	380
Bouisset	11.0	1884	1698	0.359	0.561	52.1	200

Table 4. Experimental program.

Material	Test name	Test stages	Used for
Nagen	SAT-N (saturated)	A–B: isotropic loading $p - u_w = 3 \rightarrow 240$ kPa	Validation
	1N (unsaturated)	A–B: isotropic loading $p_{net} = 20 \rightarrow 680$ kPa at constant water content after initial equalisation at $s_0 = 210$ kPa	Calibration
		B–C: unloading $p_{net} = 680 \rightarrow 20$ kPa at constant suction $s = 210$ kPa	
	2N (unsaturated)	A–B: isotropic loading $p_{net} = 20 \rightarrow 560$ kPa at constant water content after initial equalisation at $s_0 = 550$ kPa	Calibration
		B–C: unloading $p_{net} = 560 \rightarrow 20$ kPa at constant suction $s = 330$ kPa	
	3N (unsaturated)	A–B: isotropic loading $p_{net} = 20 \rightarrow 850$ kPa at constant suction $s = 50$ kPa	Validation
		B–C: unloading $p_{net} = 850 \rightarrow 20$ kPa at constant suction $s = 50$ kPa	
Bouisset	SAT-B (saturated)	A–B: isotropic loading $p - u_w = 4 \rightarrow 240$ kPa	Validation
	1B (unsaturated)	A–B: isotropic loading $p_{net} = 20 \rightarrow 830$ kPa at constant water content after initial equalisation at $s_0 = 220$ kPa	Calibration
		B–C: unloading $p_{net} = 830 \rightarrow 20$ kPa at constant suction $s = 55$ kPa	
	2B (unsaturated)	A–B: isotropic loading $p_{net} = 30 \rightarrow 790$ kPa at constant water content after initial equalisation at $s_0 = 500$ kPa	Calibration
		B–C: unloading $p_{net} = 790 \rightarrow 20$ kPa at constant suction $s = 90$ kPa	
	3B (unsaturated)	A–B: isotropic loading $p_{net} = 20 \rightarrow 500$ kPa at constant suction $s = 220$ kPa	Validation
		B–C: wetting $s = 220 \rightarrow 5$ kPa at constant mean net stress $p_{net} = 500$ kPa	
		C–D: isotropic unloading $p_{net} = 500 \rightarrow 20$ kPa at constant suction $s = 5$ kPa	
	4B (unsaturated)	A–B: isotropic loading $p_{net} = 20 \rightarrow 500$ kPa at constant suction $s = 350$ kPa	Validation
		B–C: wetting $s = 350 \rightarrow 5$ kPa at constant mean net stress $p_{net} = 500$ kPa	
		C–D: unloading $p_{net} = 500 \rightarrow 150$ kPa at constant suction $s = 5$ kPa	
		D–E: drying $s = 5 \rightarrow 100$ kPa at constant mean net stress $p_{net} = 150$ kPa	

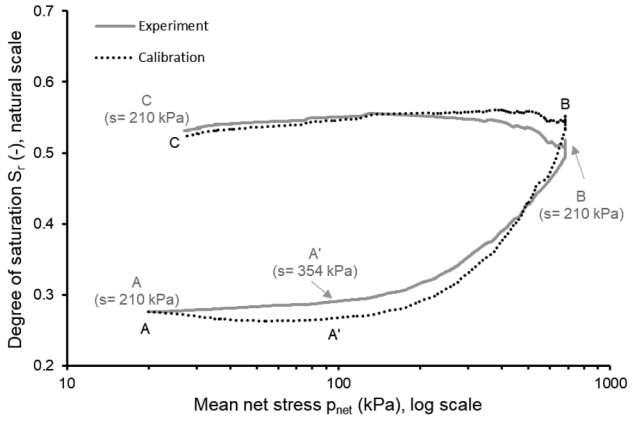

Fig. 2. Calibration of retention law against test 1N.

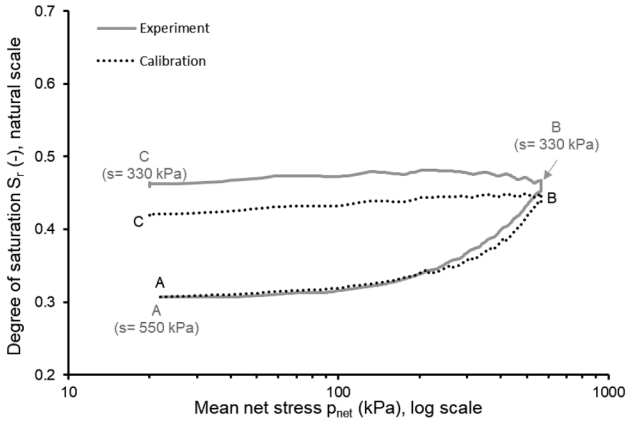

Fig. 3. Calibration of retention law against test 2N.

drying equation of Table 1 depending on the sign of the variation of the scaled suction $\bar{s} = se^{1/\lambda_s}$ defined by Gallipoli et al. (2015). A reduction of scaled suction corresponds to a wetting path (i.e., increase of degree of saturation), while an increase of scaled suction corresponds to a drying path (i.e., decrease of degree of saturation). As customary during calibration, experimental, rather than computed, values of suction and void ratio were used for calculating the scaled suction. This ensured that the calibrated curves are entirely the product of the retention law with no influence of the mechanical law. Note that the value of scaled suction varies during both loading at constant water content and unloading at constant suction because it depends on both suction and void ratio.

The constant of integration C_w of the first wetting path was calculated by matching the experimental and calibrated curves at the start of the test to avoid that a poor prediction of the initial state of the soil would compromise the quality of calibration. Instead, the constant of integration C_d of the subsequent drying path was calculated by imposing the continuity of predictions at the reversal point of the cycle. In general, Figs. 2–5 show a good agreement between experimental and calibrated values of degree

Fig. 4. Calibration of retention law against test 1B.

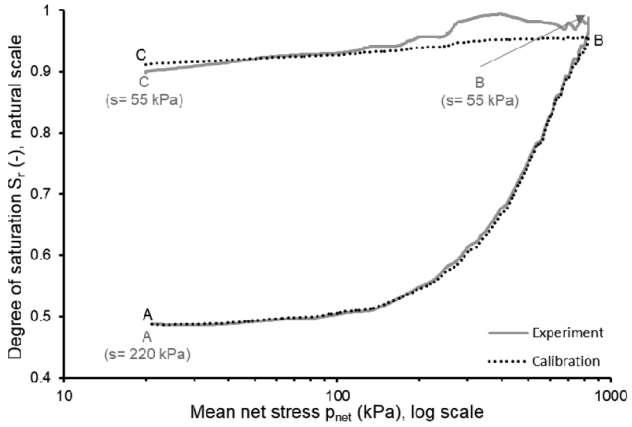

Fig. 5. Calibration of retention law against test 2B.

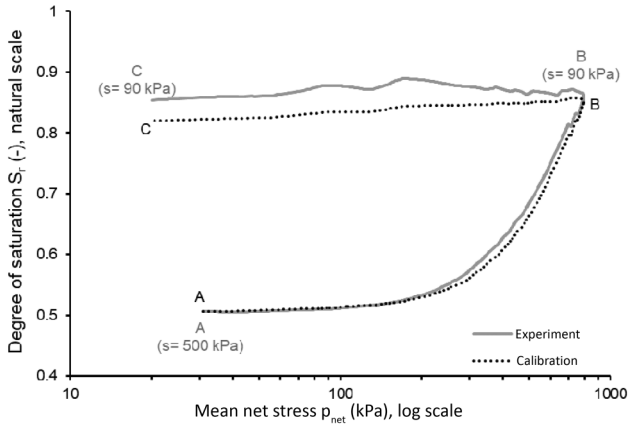

Fig. 6. Calibration of mechanical law against test 1N.

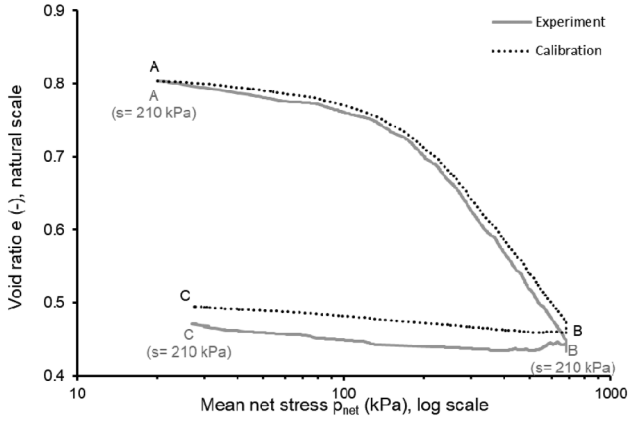

of saturation, which confirms the ability of the chosen material parameters to capture the retention behaviour of both Nagen and Bouisset soils. During constant water content loading in test 1N (Fig. 2), the model predicts a slight decrease of degree of saturation from 0.28 (point A) to 0.26 (point A′) followed by a substantial increase to 0.55 (point B), whereas the experiment indicates a

Fig. 7. Calibration of mechanical law against test 2N.

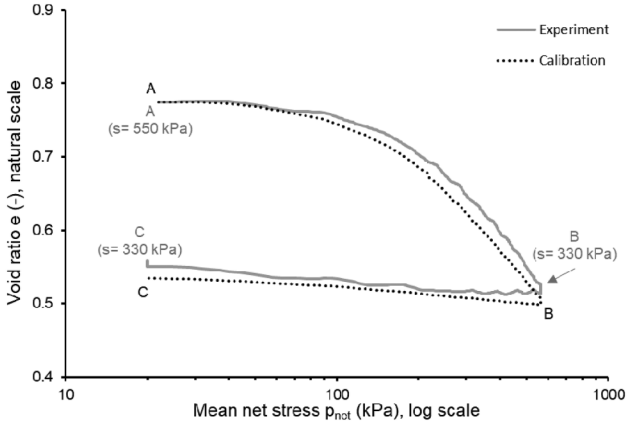

Fig. 8. Calibration of mechanical law against test 1B.

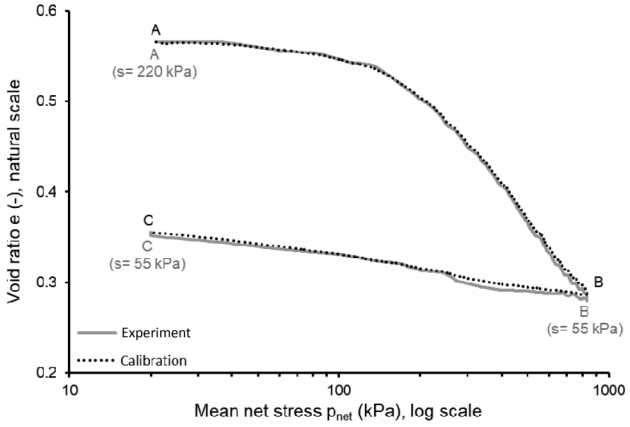

monotonic increase of degree of saturation. As discussed earlier, this small discrepancy is caused by the unrealistic measurement of an increase of suction at the start of loading, probably produced by the formation of air bubbles in the pore water line. This suction increase is interpreted by the model as drying, which produces the irregular prediction of degree of saturation during loading.

Calibration of mechanical law

The five mechanical parameters (i.e., λ_p, $\overline{p}_{ref}$, λ_r, k, and γ) were selected at once via a least square regression of the same four tests used for calibrating the retention law, i.e., tests 1N and 2N for the Nagen soil (Figs. 6 and 7) and tests 1B and 2B for the Bouisset soil (Figs. 8 and 9).

The calibrated curves were computed by using either the loading or unloading equation of Table 1 depending on the sign of the variation of the mean scaled stress $\overline{p} = p' S_r^{\lambda_r/\lambda_p}$ defined by Gallipoli and Bruno (2017). An increase of mean scaled stress corresponds to a loading path (i.e., decrease of void ratio), while a decrease of mean scaled stress corresponds to an unloading path (i.e., increase of void ratio). Experimental, rather than computed, values of degree of saturation were considered for calculating the mean scaled stress, which ensured that the calibrated curves are entirely the product of the mechanical law with no influence of the retention law.

Like the retention law, the constant of integration C_l of the first loading path was calculated by matching measured and calibrated curves at the start of the test, while the constant of integration C_u of the subsequent unloading path was calculated by imposing the continuity of the predictions at the reversal point

Fig. 9. Calibration of mechanical law against test 2B.

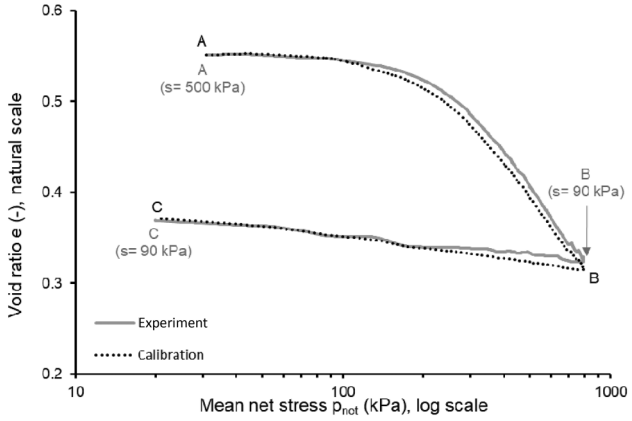

Table 5. Values of model parameters.

	Nagen	Bouisset
Retention parameters		
λ_s	0.214	0.088
ω_w (kPa)	0.275	3.58×10^{-5}
m_w	0.038	0.062
β_w	0.608	0.206
ω_d (kPa)	26 598	41 633
m_d	0.038	0.062
β_d	0.010	0.035
Mechanical parameters		
λ_r	0.539	0.728
λ_p	0.220	0.164
$\overline{p}_{ref}$ (kPa)	4.72	0.410
γ	2.05	1.23
κ	0.050	0.075

Fig. 10. Model validation against test 3N: (*a*) void ratio vs mean net stress and (*b*) degree of saturation vs mean net stress.

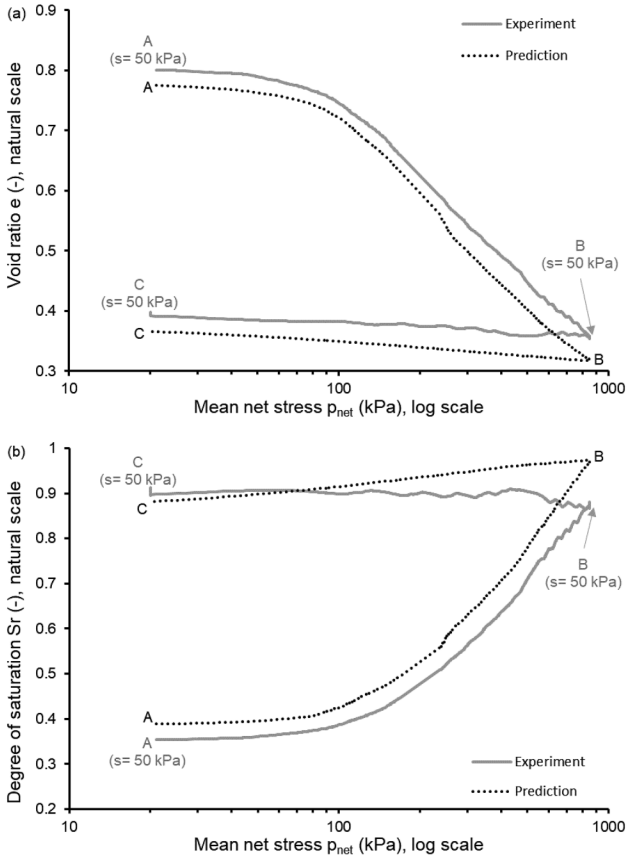

of the cycle. Inspection of Figs. 6–9 confirms that the calibrated curves accurately reproduce the mechanical behaviour of both soils, thus confirming the suitability of the chosen parameter values. The selected parameter values for both retention and mechanical laws are summarised in Table 5.

Validation of coupled hydromechanical model

The calibrated retention and mechanical laws were coupled via the previously described iterative algorithm so that the degree of saturation calculated by the retention law contributes to the computation of the void ratio by the mechanical law and vice versa. The resulting hydromechanical model was validated by predicting the degree of saturation and void ratio along stress paths, formulated in terms of suction and mean net stress, of additional tests not used during previous calibration.

To probe deeper into the model, the initial constants of integration of each test were calculated by matching predicted and measured data in correspondence of the "as-compacted" soil state (Table 3) instead of the equalised soil state at the start of the test. Therefore, unlike calibration, the initial equalised state is now predicted by the model rather than imposed, which also means that the predicted and experimental curves of each test do not start from the same point. This approach constitutes a stricter assessment of the model performance, which can no longer rely on the perfect match between predictions and experiments at the start of the test.

For the Nagen soil, model predictions were validated against results from test 3N (Table 4), which consists in a cycle of mean net stress from 20 to 850 kPa and back to 20 kPa at a constant suction of 50 kPa. Figures 10 shows a generally good agreement between experimental and predicted curves of both void ratio and degree of saturation. Note also that test 3N was performed at a constant suction of 50 kPa, which is lower than the suction range explored during calibration. This result, therefore, indicates the ability of the model to extrapolate predictions beyond the original experimental data.

For the Bouisset soil, model predictions were validated against two tests, i.e., 3B and 4B, which involved cyclic variations of mean net stress and suction (Table 4). Both tests start with an increase of mean net stress from 20 to 500 kPa at constant suction of 220 kPa, for test 3B, and 350 kPa, for test 4B. Suction is then decreased to 5 kPa in both tests at a constant mean net stress of 500 kPa, followed by a reduction of mean net stress to 20 kPa, for test 3B, and 150 kPa, for test 4B, at a constant suction of 5 kPa. Finally, test 4B undergoes an increase of suction from 5 to 100 kPa at a constant mean net stress of 150 kPa.

Figures 11 and 12 show generally good predictions of degree of saturation and void ratio under varying levels of mean net stress and suction, including a relatively accurate prediction of degree of saturation and volumetric collapse after the rest periods at the end of the suction reduction stages (i.e., stage B–C in Figs. 11 and 12). The discrepancies between experiments and predictions along wetting paths are mostly due to the relatively high suction reduction rate (2 kPa/h) during experiments, which was too fast to allow the equalisation of pore water pressure inside the sample. This is confirmed by the significant increase of degree of saturation, and the associated decrease of void ratio, during the rest

Fig. 11. Model validation against test 3B: (*a*) void ratio vs mean net stress, (*b*) void ratio vs suction, and (*c*) degree of saturation vs suction.

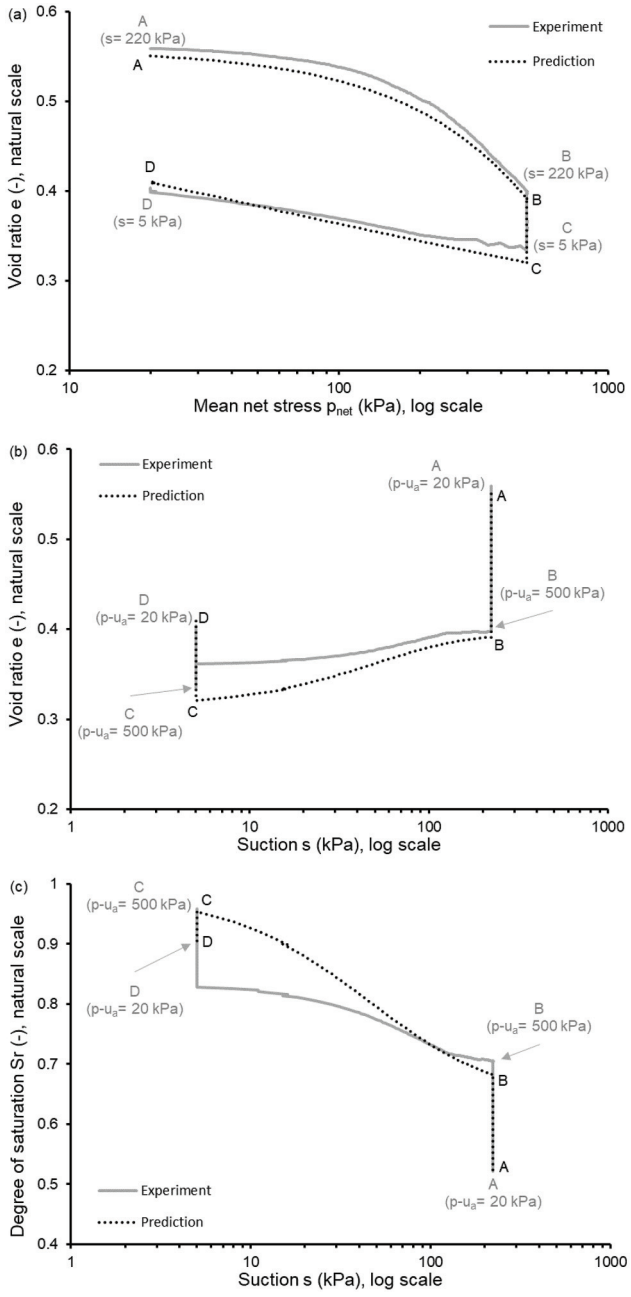

Fig. 12. Model validation against test 4B: (*a*) void ratio vs mean net stress, (*b*) void ratio vs suction, and (*c*) degree of saturation vs suction.

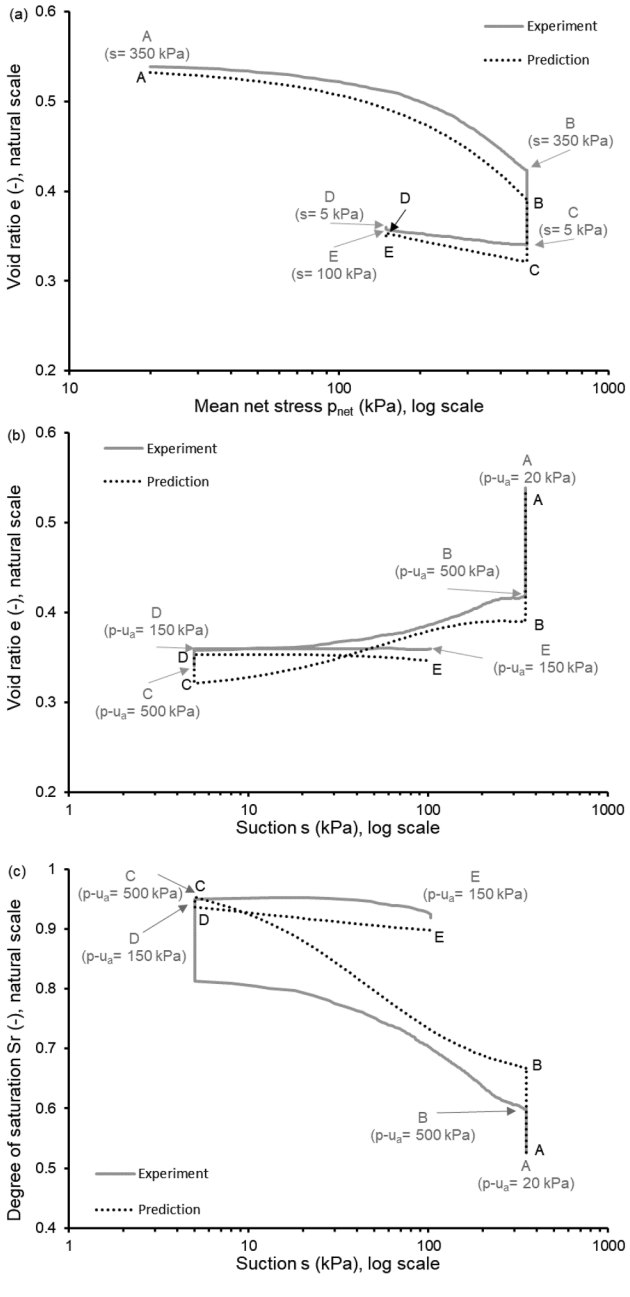

periods at the end of the suction reduction stages. With the benefit of hindsight, a slower suction reduction rate should have been imposed, or at least, suction should have been measured at the sample mid-height by means of high-capacity tensiometers to cross-check equalisation inside the soil. Note that the wetting-induced collapse of compacted or reconstituted samples may not be fully representative of the behaviour of undisturbed collapsible soils. This aspect is, however, outside the scope of the present paper and will constitute matter for future research.

Figure 13 shows the results from two saturated tests, i.e., test SAT-N on Nagen soil and test SAT-B on Bouisset soil (Table 4), together with the corresponding model prediction. Note that the soil state at the start of both tests was predicted by the model via the simulation of the initial saturation of the sample under a low confining pressure of about 5 kPa. Inspection of Fig. 13 indicates that, in both cases, the model successfully predicts the full saturation and swelling of the sample as suction changes from the value after compaction to zero. Importantly, the same model parameters determined from unsaturated tests (i.e., tests 1N and 2N for Nagen soil or tests 1B and 2B for Bouisset soi; see section on mechanical calibration) provide an excellent match also to the two saturated tests. This confirms the ability of the model to predict soil deformations regardless of the saturation state of the soil, which corroborates the unifying modelling approach of Gallipoli and Bruno (2017).

Fig. 13. Model validation against the saturated tests SAT-N and SAT-B performed on Nagen and Bouisset soils, respectively. [Colour online.]

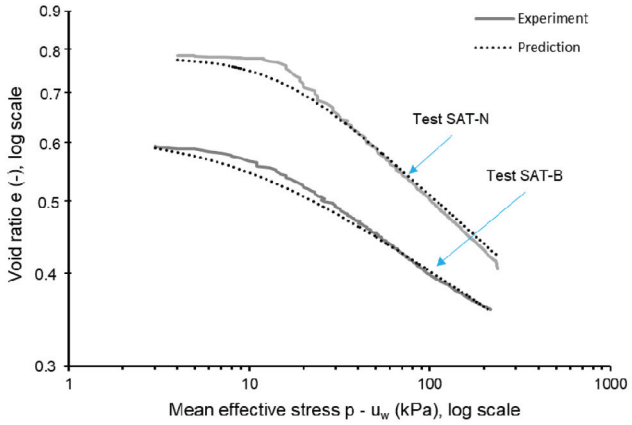

Conclusions

This paper has presented original data from a series of unsaturated and saturated isotropic tests performed on compacted samples of a sandy silt (Nagen soil) and a clayey silt (Bouisset soil) inside triaxial cells. The tests involved either an increase or a decrease of mean net stress at constant suction or an increase or a decrease of suction at constant mean net stress. Some samples were also subjected to an increase of mean net stress at constant water content with the simultaneous measurement of suction. During all tests, the void ratio and the degree of saturation were continuously recorded to assess the mechanical and retention behaviour of the soils. Test results were subsequently used for the calibration and validation of the bounding surface hysteretic hydromechanical model of Bruno and Gallipoli (2019). The main findings can be summarised as follows:

- Loading at constant water content with measurement of suction is highly convenient for model calibration because it allows the simultaneous exploration of relatively large ranges of mean net and suction via a limited number of fast tests.
- The model reproduces well the unsaturated hydromechanical behaviour of both sandy silt and clayey silt tested in this work. This result also extends the previous validation of the model, which was limited to finer soils from bentonitic and kaolinitic clays to loess silts.
- The progressive yielding and smooth retention response of the soils are well captured by the adopted bounding surface model.
- The model correctly predicts the magnitude of volumetric collapse and saturation during wetting at constant mean net stress, though some discrepancies exist due to the relatively high rate of suction reduction imposed during the tests.
- The saturated behaviour of the two soils is accurately reproduced by the model using the parameters selected by fitting only unsaturated tests. This corroborates the efficacy of the scaled constitutive variables in unifying the behaviour of saturated and unsaturated soils within a single material framework.

Future work will focus on extending the validation of the hydromechanical model to intact or undisturbed soils.

References

AFNOR. 1991. Soils: investigation and testing. Determination of particle density. Pycnometer method. NF P94-054.

AFNOR. 1992. Soils: investigation and testing. Granulometric analysis. Hydrometer method. NF P94-057.

AFNOR. 1993. Soils: investigation and testing. Determination of Atterberg's limits. Liquid limit test using Casagrande apparatus. Plastic limit test on rolled thread. NF P94-051.

AFNOR. 1995*a*. Soils: investigation and testing. Determination of moisture content. Oven drying method. NF P94-050.

AFNOR. 1995*b*. Soils: investigation and testing. Granulometric description. Wet sieving method. XP P94-041.

Al-Sharrad, M.A. 2013. Evolving anisotropy in unsaturated soils: experimental investigation and constitutive modelling. Doctoral dissertation, University of Glasgow.

Alonso, E.E., Gens, A., and Josa, A. 1990. A constitutive model for partially saturated soils. Géotechnique, **40**(3): 405–430. doi:10.1680/geot.1990.40.3.405.

Balzano, B., Bruno, A.W., Denzer, H., Molan, D., Tarantino, A., and Gallipoli, D. 2021. REAL-TIME quality check of measurements of soil water status in the vadose zone. Physics and Chemistry of the Earth, Parts A/B/C, **121**: 102918. doi:10.1016/j.pce.2020.102918.

Bruno, A.W., and Gallipoli, D. 2019. A coupled hydromechanical bounding surface model predicting the hysteretic behaviour of unsaturated soils. Computers and Geotechnics, **110**: 287–295. doi:10.1016/j.compgeo.2019.02.025.

Bruno, A.W., Gallipoli, D., Perlot, C., and Mendes, J. 2017. Mechanical behaviour of hypercompacted earth for building construction. Materials and Structures, **50**(2): 160. doi:10.1617/s11527-017-1027-5.

Casini, F., Vaunat, J., Romero, E., and Desideri, A. 2012. Consequences on water retention properties of double-porosity features in a compacted silt. Acta Geotechnica, **7**(2): 139–150. doi:10.1007/s11440-012-0159-6.

Cuccurullo, A., Gallipoli, D., Bruno, A.W., Augarde, C.E., Hughes, P., and La Borderie, C. 2018. Influence of soil grading on the hygro-mechanical properties of hyper-compacted earth for masonry construction. *In* Proceedings of the 10th International Masonry Conference (10 IMC), Milano, Italy, 9–11 July 2018. pp. 1459–1471.

Cunningham, M.R., Ridley, A.M., Dineen, K., and Burland, J.B. 2003. The mechanical behaviour of a reconstituted unsaturated silty clay. Géotechnique, **53**(2): 183–194. doi:10.1680/geot.2003.53.2.183.

Delage, P., Audiguier, M., Cui, Y.J., and Howat, M.D. 1996. Microstructure of a compacted silt. Canadian Geotechnical Journal, **33**(1): 150–158. doi:10.1139/t96-030.

Delage, P., Howat, M.D., and Cui, Y.J. 1998. The relationship between suction and swelling properties in a heavily compacted unsaturated clay. Engineering Geology, **50**(1–2): 31–48. doi:10.1016/S0013-7952(97)00083-5.

Fredlund, D.G., and Wong, D.K. 1989. Calibration of thermal conductivity sensors for measuring soil suction. Geotechnical Testing Journal, **12**(3): 188–194. doi:10.1520/GTJ10967J.

Fredlund, D.G., and Xing, A. 1994. Equations for the soil-water characteristic curve. Canadian Geotechnical Journal, **31**(4): 521–532. doi:10.1139/t94-061.

Gallipoli, D., and Bruno, A.W. 2017. A bounding surface compression model with a unified virgin line for saturated and unsaturated soils. Géotechnique, **67**(8): 703–712. doi:10.1680/jgeot.16.P.145.

Gallipoli, D., Wheeler, S.J., and Karstunen, M. 2003*a*. Modelling the variation of degree of saturation in a deformable unsaturated soil. Géotechnique, **53**(1): 105–112. doi:10.1680/geot.2003.53.1.105.

Gallipoli, D., Gens, A., Sharma, R., and Vaunat, J. 2003*b*. An elasto-plastic model for unsaturated soil incorporating the effects of suction and degree of saturation on mechanical behaviour. Géotechnique, **53**(1): 123–136. doi:10.1680/geot.2003.53.1.123.

Gallipoli, D., Bruno, A.W., D'onza, F., and Mancuso, C. 2015. A bounding surface hysteretic water retention model for deformable soils. Géotechnique, **65**(10): 793–804. doi:10.1680/jgeot.14.P.118.

Gan, J.K.M., Fredlund, D.G., and Rahardjo, H. 1988. Determination of the shear strength parameters of an unsaturated soil using the direct shear test. Canadian Geotechnical Journal, **25**(3): 500–510. doi:10.1139/t88-055.

Geiser, F., Laloui, L., and Vulliet, L. 2006. Elasto-plasticity of unsaturated soils: laboratory test results on a remoulded silt. Soils and Foundations, **46**(5): 545–556. doi:10.3208/sandf.46.545.

Jotisankasa, A., Ridley, A., and Coop, M. 2007. Collapse behavior of compacted silty clay in suction-monitored oedometer apparatus. Journal of Geotechnical and Geoenvironmental Engineering, ASCE, **133**(7): 867–877. doi:10.1061/(ASCE)1090-0241(2007)133:7(867).

Khalili, N., Habte, M.A., and Zargarbashi, S. 2008. A fully coupled flow deformation model for cyclic analysis of unsaturated soils including hydraulic and mechanical hystereses. Computers and Geotechnics, **35**(6): 872–889. doi:10.1016/j.compgeo.2008.08.003.

Lim, B.F., and Siemens, G.A. 2016. Unifying framework for modeling swelling soil behaviour. Canadian Geotechnical Journal, **53**(9): 1495–1509. doi:10.1139/cgj-2015-0049.

Lloret-Cabot, M., Sánchez, M., and Wheeler, S.J. 2013. Formulation of a three-dimensional constitutive model for unsaturated soils incorporating mechanical–water retention couplings. International Journal for Numerical and Analytical Methods in Geomechanics, **37**(17): 3008–3035. doi:10.1002/nag.2176.

Lloret-Cabot, M., Wheeler, S.J., and Sánchez, M. 2017. A unified mechanical and retention model for saturated and unsaturated soil behaviour. Acta Geotechnica, **12**(1): 1–21. doi:10.1007/s11440-016-0497-x.

Lloret-Cabot, M., Wheeler, S.J., Pineda, J.A., Romero, E., and Sheng, D. 2018. From saturated to unsaturated conditions and vice versa. Acta Geotechnica, **13**(1): 15–37. doi:10.1007/s11440-017-0577-6.

Lourenço, S.D.N., Gallipoli, D., Toll, D.G., Augarde, C.E., Evans, F.D., and Medero, G.M. 2008. Calibrations of a high-suction tensiometer. Géotechnique, **58**(8): 659–668. doi:10.1680/geot.2008.58.8.659.

Lourenço, S.D.N., Gallipoli, D., Toll, D.G., Augarde, C.E., and Evans, F.D. 2011. A new procedure for the determination of the soil–water retention curves by continuous drying using high-suction tensiometers. Canadian Geotechnical Journal, **48**(2): 327–335. doi:10.1139/T10-062.

Mendes, J., Toll, D.G., Augarde, C.E., and Gallipoli, D. 2008. A system for field measurement of suction using high capacity tensiometers. *In* Unsaturated Soils. Advances in Geo-Engineering. *Edited by* D.G. Toll, C.E. Augarde, D. Gallipoli, and S.J. Wheeler. CRC Press. pp. 219–225.

Mendes, J., Gallipoli, D., Tarantino, A., and Toll, D. 2019. On the development of an ultra-high-capacity tensiometer capable of measuring water tensions to 7 MPa. Géotechnique, **69**(6): 560–564. doi:10.1680/jgeot.18.T.008.

Monroy, R., Zdravkovic, L., and Ridley, A. 2010. Evolution of microstructure in compacted London Clay during wetting and loading. Géotechnique, **60**(6): 105–119. doi:10.1680/geot.8.P.125.

Nuth, M., and Laloui, L. 2008. Advances in modelling hysteretic water retention curve in deformable soils. Computers and Geotechnics, **35**(6): 835–844. doi:10.1016/j.compgeo.2008.08.001.

Oka, F., Kodaka, T., Suzuki, H., Kim, Y.S., Nishimatsu, N., and Kimoto, S. 2010. Experimental study on the behavior of unsaturated compacted silt under triaxial compression. Soils and Foundations, **50**(1): 27–44. doi:10.3208/sandf.50.27.

Raveendiraraj, A. 2009. Coupling of mechanical behaviour and water retention behaviour in unsaturated soils. Doctoral dissertation, University of Glasgow.

Ridley, A.M., and Burland, J.B. 1993. A new instrument for the measurement of soil moisture suction. Géotechnique, **43**(2): 321–324. doi:10.1680/geot.1993.43.2.321.

Romero, E., Della Vecchia, G., and Jommi, C. 2011. An insight into the water retention properties of compacted clayey soils. Géotechnique, **61**(4): 313–328. doi:10.1680/geot.2011.61.4.313.

Sharma, R.S. 1998. Mechanical behaviour of unsaturated highly expansive clays. Doctoral dissertation, University of Oxford.

Siemens, G.A., Take, W.A., and Peters, S.B. 2014. Physical and numerical modeling of infiltration including consideration of the pore-air phase. Canadian Geotechnical Journal, **51**(12): 1475–1487. doi:10.1139/cgj-2013-0447.

Sivakumar, V. 1993. A critical state framework for unsaturated soil. Doctoral dissertation, University of Sheffield.

Skempton, A.W. 1953. The colloidal "Activity" of clays. *In* Selected Papers on Soil Mechanics. pp. 106–118.

Sun, D.A., Sheng, D., Xiang, L., and Sloan, S.W. 2008. Elastoplastic prediction of hydro-mechanical behaviour of unsaturated soils under undrained conditions. Computers and Geotechnics, **35**(6): 845–852. doi:10.1016/j.compgeo.2008.08.002.

Sun, D.A., Zhang, J., Gao, Y., and Sheng, D. 2016. Influence of suction history on hydraulic and stress-strain behavior of unsaturated soils. International Journal of Geomechanics, ASCE, **16**(6): D4015001. doi:10.1061/(ASCE)GM.1943-5622.0000602.

Tarantino, A. 2009. A water retention model for deformable soils. Géotechnique, **59**(9): 751–762. doi:10.1680/geot.7.00118.

Tarantino, A., and De Col, E. 2008. Compaction behaviour of clay. Géotechnique, **58**(3): 199–213. doi:10.1680/geot.2008.58.3.199.

Tarantino, A., and Tombolato, S. 2005. Coupling of hydraulic and mechanical behaviour in unsaturated compacted clay. Géotechnique, **55**(4): 307–317. doi:10.1680/geot.2005.55.4.307.

Tatsuoka, F. 2015. Compaction characteristics and physical properties of compacted soil controlled by the degree of saturation. *In* Deformation Characteristics of Geomaterials: Proceedings of the 6th International Symposium on Deformation Characteristics of Geomaterials, IS-Buenos Aires 2015, Buenos Aires, Argentina, 15–18 November 2015. pp. 40–78.

Tinjum, J.M., Benson, C.H., and Blotz, L.R. 1997. Soil-water characteristic curves for compacted clays. Journal of Geotechnical and Geoenvironmental Engineering, ASCE, **123**(11): 1060–1069. doi:10.1061/(ASCE)1090-0241(1997)123:11(1060).

Toll, D.G., Lourenço, S.D., and Mendes, J. 2013. Advances in suction measurements using high suction tensiometers. Engineering Geology, **165**: 29–37. doi:10.1016/j.enggeo.2012.04.013.

Van Genuchten, M.T. 1980. A closed-form equation for predicting the hydraulic conductivity of unsaturated soils. Soil Science Society of America Journal, **44**(5): 892–898. doi:10.2136/sssaj1980.03615995004400050002x.

Wheeler, S.J., and Sivakumar, V. 1995. An elasto-plastic critical state framework for unsaturated soil. Géotechnique, **45**(1): 35–53. doi:10.1680/geot.1995.45.1.35.

Wheeler, S.J., Sharma, R.S., and Buisson, M.S.R. 2003. Coupling of hydraulic hysteresis and stress–strain behaviour in unsaturated soils. Géotechnique, **53**(1): 41–54. doi:10.1680/geot.2003.53.1.41.

Zhao, H.F., and Zhang, L.M. 2014. Effect of coarse content on shear behavior of unsaturated coarse granular soils. Canadian Geotechnical Journal, **51**(12): 1371–1383. doi:10.1139/cgj-2012-0292.

Zhou, A., Wu, S., Li, J., and Sheng, D. 2018. Including degree of capillary saturation into constitutive modelling of unsaturated soils. Computers and Geotechnics, **95**: 82–98. doi:10.1016/j.compgeo.2017.09.017.